Electronic structure and vacancy formation in photochromic yttrium oxy-hydride thin films studied by positron annihilation

Plokker, M. P.; Eijt, S. W H; Naziris, F.; Schut, H.; Nafezarefi, F.; Schreuders, H.; Cornelius, S.; Dam, B.

DOI
10.1016/j.solmat.2017.03.011

Publication date
2018

Document Version
Final published version

Published in
Solar Energy Materials & Solar Cells

Solar Energy Materials & Solar Cells 177 (2018) 97–105

Contents lists available at ScienceDirect

Solar Energy Materials & Solar Cells

journal homepage: www.elsevier.com/locate/solmat

Electronic structure and vacancy formation in photochromic yttrium oxy-hydride thin films studied by positron annihilation

M.P. Plokker[a], S.W.H. Eijt[a,*], F. Naziris[a], H. Schut[b], F. Nafezarefi[c], H. Schreuders[c], S. Cornelius[c], B. Dam[c]

[a] Fundamental Aspects of Materials and Energy, Department of Radiation Science and Technology, Faculty of Applied Sciences, Delft University of Technology, Mekelweg 15, NL-2629 JB Delft, The Netherlands
[b] Neutron and Positron Methods in Materials, Department of Radiation Science and Technology, Faculty of Applied Sciences, Delft University of Technology, Mekelweg 15, NL-2629 JB Delft, The Netherlands
[c] Materials for Energy Conversion and Storage, Department of Chemical Engineering, Faculty of Applied Sciences, Delft University of Technology, Van der Maasweg 9, NL-2629 HZ Delft, The Netherlands

ARTICLE INFO

Keywords:
Photochromic materials
Vacancies
Electronic structure
Yttrium hydride
Positron annihilation
Thin films

ABSTRACT

In order to investigate the mechanism of the photochromic effect in yttrium oxy-hydride (YO_xH_y) thin films, Doppler broadening positron annihilation spectroscopy (PAS) was applied to probe the electronic structure and the presence of vacancies in YO_xH_y and related materials as a function of composition, UV illumination and thermal annealing. The Doppler S and W parameter depth profiles of a series of Y, yttrium di-hydride $YH_{1.9+\delta}$ and Y_2O_3 thin films show strong systematic changes caused by the distinct differences in electronic structure of the metals Y, $YH_{1.9+\delta}$ and the wide band gap insulator Y_2O_3. The Doppler broadening parameters of photochromic YO_xH_y (a semiconductor with a band gap of ~2.6 eV) are intermediate to those of $YH_{1.9+\delta}$ and Y_2O_3. In order to probe the nanostructural changes related to the photochromic effect, the S parameter of YO_xH_y was monitored during in-situ UV illumination. A small but systematic increase of the S parameter was observed, possibly induced by generation of cation mono-vacancies or small vacancy clusters involving generated anion vacancies. The changes did not relax during bleaching under dark conditions, showing that the structural changes are not directly responsible for the photochromic mechanism. For temperatures above around 90 °C, thermal annealing leads to a substantial increase in the Doppler S parameter, pointing to the formation of vacancies by local removal of hydrogen. Simultaneously, the optical band gap increases, consistent with an increase in O:H ratios.

1. Introduction

Inorganic materials such as the transition metal oxides WO_3 and MoO_3 show a photochromic effect [1] where visible or ultraviolet (UV) illumination leads to a coloration of the initially transparent films, closely related to that observed in the field of electrochromic materials [1–4]. In the latter, the coloration is linked to the insertion of H^+ or Li^+ ions, introducing additional electronic states within the forbidden gap which act as coloration centers [2,4].

On the other hand, metal hydrides are known for their remarkable switchable optical properties which can be tuned by changing the concentration of hydrogen inserted into the lattice. The discovery of large reversible changes in resistivity and optical transmission of yttrium films upon hydrogenation from the gas phase by Huiberts *et al.* [5,6] marked the start of intensive research of metal-insulator transitions in (rare-earth) metal hydrides. The large changes in optical transmittance can be exploited in applications such as smart windows, including all-solid state switchable windows, and hydrogen sensors [7].

The metal-insulator transition in the YH_x system occurs upon hydrogenation into the hexagonal $YH_{3-\varepsilon}$ phase for compositions around $YH_{\sim 2.86}$, and is caused by the opening of an indirect optical band gap close to 3 eV, as was revealed by ab-initio calculations of the electronic band structure employing the GW approximation [8]. The metallic fcc $YH_{1.9+\delta}$ phase also shows intriguing optical properties, with a characteristic transmittance window in the range of 1.5–2.0 eV [9]. Remarkably, UV illumination of yttrium hydride YH_x leads to persis-

* Corresponding author.
E-mail address: s.w.h.eijt@tudelft.nl (S.W.H. Eijt).

http://dx.doi.org/10.1016/j.solmat.2017.03.011
Received 16 January 2017; Received in revised form 6 March 2017; Accepted 12 March 2017
Available online 23 March 2017

tent photoconductivity [10]. Hoekstra et al. [10] attributed the stability of the generated free charge carriers up to 200 K to subtle rearrangements of hydrogen. Ohmura et al. [11] found that yttrium hydride in fact shows reversible photochromic behaviour under laser illumination at room temperature, albeit at high pressures of the order of 5 GPa.

In 2011, Mongstad *et al.* [12,13] discovered that oxygen containing transparent yttrium hydride (YO_xH_y) films, stabilized in the $YH_{1.9+\delta}$ like fcc crystal structure, show a remarkable and reversible persistent photoconductivity and photochromic effect upon illumination with UV light under ambient conditions. The reported YO_xH_y films are transparent with an indirect band gap of ~2.6 eV, and show color-neutral photo-darkening for oxygen concentrations in the range of around 5–30%, while they bleach reversibly under dark conditions at room temperature [12]. The induced persistent photoconductivity indicates that charge carrier generation is a key component in the photochromism. However, Nuclear Magnetic Resonance (NMR) studies showed that local hydrogen rearrangements are also involved, since a 3% mobile hydrogen fraction was seen to "freeze out" upon photo-darkening, and the mobile H reappeared during bleaching under dark conditions [14]. Theoretical simulations further indicated the importance of oxygen to stabilize the $YH_{1.9+\delta}$ like fcc crystal structure and oxygen may lead to additional charge transfer due to its higher electronegativity, in which the local Y^{2+}/Y^{3+} valence ratio is modified by replacement of hydrogen by oxygen [15]. The optical band gap can be tailored in the range 2.6–3.7 eV by tuning the deposition pressure during magnetron sputter deposition leading to increased oxygen incorporation in the YO_xH_y films [16].

In this study, we applied Doppler broadening positron annihilation spectroscopy (PAS) with a threefold aim to gain better insights into these remarkable properties of photochromic yttrium oxy-hydride films. In contrast to surface sensitive techniques like X-ray photoelectron spectroscopy, PAS offers the possibility to probe the electronic structure selectively within the film without any surface contribution, by tuning the mean positron implantation depth.

First, we applied PAS to investigate electronic structure properties of thin films of the metals Y and $YH_{1.9+\delta}$, the wide band gap insulator Y_2O_3 and semiconductor YO_xH_y in a depth resolved manner. Positron annihilation spectroscopy is a sensitive technique to probe the electronic structure of materials via detection of the electron momentum distribution. The Fermi surface of Y and positron-electron momentum distributions of Y were extracted in detailed positron 2D-ACAR experiments [17] and by ab-initio calculations [18]. Previous positron Doppler broadening studies on MgH_2-based films demonstrated the great sensitivity to probe the metal-insulator transition in the Mg-MgH_2 system [19–21].

Secondly, the nanostructural changes in photochromic YO_xH_y films were probed by PAS during in-situ UV illumination, since the mechanism underlying the photochromic effect in yttrium oxy-hydride films is currently not known. Here, the potential role of vacancy-related defects is investigated, making use of the high sensitivity of positron annihilation spectroscopy methods to detect and identify vacancy-related defects [22–24]. The photochromism and electrochromism of transition metal oxides is often associated with the occurrence of point defects (which act as color centers), consisting of vacancies or small vacancy-complexes with a trapped (photo-excited) electron, leading to defect states in the band gap and associated sub-band gap optical absorption. A correlation between positron annihilation lifetimes and color centers was previously established for NaCl [25], although the F centers which disappear upon optical bleaching did not form effective trapping sites for positrons. Alternatively, since Y can attain a valence of Y^{3+} or Y^{2+}, YO_xH_y films may attain a Y^{3+}/Y^{2+} mixed valence character. Therefore, intervalence charge transfer and its associated local electronic structure may also play an important role in the photochromism. In such an intervalence charge transfer model, the local binding of H is expected to play a key role in the local charge transfer and coloration of the films. A third model involves the formation of small, metallic Y or $YH_{1.9+\delta}$ clusters, where effective medium theory predicts that photo-darkening due to scattering and absorption of sub-band gap visible light can be induced by Y or $YH_{1.9+\delta}$ clusters formed in a semiconductor YO_xH_y host medium (which is transparent to sub-band gap illumination). Such ultrasmall Y or $YH_{1.9+\delta}$ clusters might be detected by positron annihilation techniques if their positron affinity is larger than that of the surrounding YO_xH_y, similar to Mg nanoclusters in TiH_2 [26], Li nanoclusters in MgO [27,28] and Cu nanoclusters in Fe [29].

Finally, as a third aim, positron annihilation studies of yttrium oxy-hydride films were performed as a function of temperature, in order to examine possible nanostructural changes and vacancy-related defect formation in the yttrium oxy-hydrides during thermal annealing.

2. Experimental methods

A series of yttrium-based thin film samples on UV-grade fused silica (f-SiO_2) substrates was prepared by reactive direct current (DC) magnetron sputtering at room temperature using an AJA ATC2400 sputter deposition system equipped with six planar cylindrical 2-in. magnetron sources and a rotating sample holder (60 rpm) operating at a base vacuum pressure of ~10^{-6} Pa. The photochromic properties of the YO_xH_y films were investigated in transmittance using a custom-built optical fibre based spectral photometer equipped with an Ocean Optics DH-2000BAL light source and an Ocean Optics HR-4000 detector operating in the spectral range of 220–1000 nm. A Bruker D8 Advance X-ray diffractometer with Co Kα X-rays (λ=1.7890 Å) was used to record X-ray diffractograms in the Bragg-Brentano focussing geometry. Yttrium thin films of 300–500 nm thickness were deposited from an yttrium target (99.9% purity) in an Ar (6N) atmosphere at 0.3 Pa and 100 W discharge power. Subsequently, these films were covered by 10 nm of Pd at the same deposition conditions. The Pd cap layer serves as an oxidation protection for the metallic Y as well as a catalyst during hydrogenation of Y to form hydride phases. The diffraction pattern of the Y film is consistent with #00-33-1458 of the International Centre for Diffraction data (ICDD) powder diffraction file (PDF) database showing a hcp crystal structure (*P*63/*mmc*), with a pronounced c-axis texture with only (002) and (004) Bragg reflections present and a c-axis parameter of c =5.75 Å.

In order to obtain yttrium di-hydride, a Pd capped Y film was exposed to 1 bar of 4% H_2 mixed in Ar at room temperature inside a UHV pressure cell (base pressure ~10^{-4} Pa). Under these conditions, initially the yttrium tri-hydride phase is formed, which is readily observed by the significant increase of the visible transmittance during hydrogenation. It is well known that the tri-hydride phase is not stable under ambient conditions. Upon exposure of the sample to air, hydrogen is released and the sample stabilizes in the $YH_{1.9+\delta}$ phase. The presence of this phase is verified by the observation of a transmittance window in the wavelength range from 500 to 1000 nm, which is characteristic for the band structure of $YH_{1.9+\delta}$ ($0 < \delta < 0.2$) [9]. XRD analysis of the Pd capped hydrogenated film after air exposure shows that the film underwent a phase transition into the fcc structure (Fm-3m) matching the ICDD-PDF pattern #04-006-6935 of yttrium di-hydride. The film is (111) textured with a lattice parameter of a =5.24 Å, demonstrating that the crystallite orientation is preserved during hydrogenation, since the hcp c-axis of Y metal is parallel to the (111) fcc axis of yttrium di-hydride. For simplicity, from here on this sample is referred to as $YH_{1.9+\delta}$ or yttrium di-hydride.

As a reference, a 500 nm thick yttrium oxide film was prepared by adding 10 vol% of O_2 (5N) to Ar at a total pressure of 0.3 Pa using a discharge power of 200 W DC. Under these conditions the magnetron discharge operates in the transition mode close to the oxidized regime, resulting in insulating highly transparent films with a direct optical bandgap of (5.6 ± 0.1) eV (derived from Tauc plot analysis) and maximum transmittance of ~93% below the bandgap. The XRD pattern analysis reveals that the sample is a mixture of the cubic bixbyite (Ia-3)

and the monoclinic polymorphs of Y_2O_3 in agreement with the ICDD-PDF patterns #00-041-1105 and #00-044-0399, respectively. The presence of dominant cubic (222) and (444) Bragg reflexes suggests preferred (111) texture.

Photochromic yttrium oxy-hydride samples were obtained in a two-step process. First, 12.5 vol% of H_2 (5N) are added to Ar at 0.5 Pa deposition pressure and 100 W DC applied to the Y target. The resulting films are directly transferred from UHV into an oxygen free (< 0.1 ppm) glovebox under Ar atmosphere equipped with an optical fibre spectrometer. The films appear dark opaque to the eye and show the characteristic $YH_{1.9+\delta}$ transmittance window mentioned above. Upon exposure of these *uncapped* Y di-hydride films to air they change within seconds from dark to pale yellowish transparent YO_xH_y. Optical transmittance confirms a phase transition to a semiconductor with an indirect band-gap of (2.55 ± 0.05) eV (derived from Tauc plot analysis). According to the XRD the material is polycrystalline without pronounced texture having an fcc cubic crystal structure that is best described by ICDD-PDF pattern #04-006-6935 of Y-dihydride, but with a larger lattice constant of a =5.39 Å. This corresponds to a lattice expansion of about 3% compared to $YH_{1.9+\delta}$ which can be attributed to the incorporation of oxygen into the lattice.

The positron Doppler broadening of the 511 keV annihilation radiation was measured using positrons with a tunable kinetic energy in the range of 0–25 keV at the Variable Energy Positron (VEP) facility located at the Reactor Institute Delft (NL). The Doppler S and W parameters were determined using momentum windows for S and W of $|p| < 3.0{\cdot}10^{-3}\ m_oc$ and $8.2{\cdot}10^{-3}\ m_oc < |p| < 23.4{\cdot}10^{-3}\ m_oc$, respectively, with m_o and c representing the electron rest mass and the velocity of light in vacuum. The S parameter is a measure of positron annihilation with valence electrons, which provides sensitivity to the electronic structure and the presence of open volume defects such as vacancies or vacancy clusters. The increase in concentration or size of vacancies or vacancy clusters in an otherwise identical material generally leads to an increase of the S parameter. The W parameter is a measure of annihilation with (semi-)core electrons which provides chemical sensitivity to the positron trapping site. The S and W depth profiles were analyzed using the VEPFIT program [30]. The detailed procedures for the positron Doppler broadening depth profiling method is described in Ref. [31].

2.1. In-situ illumination positron annihilation studies

For the in-situ positron annihilation studies under UV illumination, a batch of YO_xH_y films with a thickness of 460 nm was prepared in the same deposition run.

Fig. 1 presents a schematic drawing of the modified sample chamber of the VEP-facility used in the in-situ PAS depth profiling studies during photo-darkening and bleaching. For photo-darkening, a HeroLab UV-6 S/L low pressure mercury lamp with emission lines centered at λ=254 nm and λ=365 nm was used. Using an Ocean Optics USB-2000+ photodetector calibrated for absolute irradiance measurements, the total UV-irradiance at the sample position in this geometrical configuration is found to be (590 ± 50) μW/cm^2. In comparison, the integrated UV-irradiance of the standard AM1.5 solar spectrum is 4610 μW/cm^2 in the same wavelength range as the UV-6 S/L lamp (245 nm < λ < 400 nm) [44].

Apart from studies of the S(E) and W(E) depth profiles, experiments were performed to collect the S and W parameter at a single positron implantation energy (constant mean implantation depth) as a function of time during illumination and subsequent bleaching under dark conditions. In order to determine the optimum positron implantation energy for each sample, simulations were performed, to find the maximum overlap of the energy dependent Makhovian positron implantation depth profile [30,31] and the UV-light intensity depth profile. The latter was obtained from a simple Lambert-Beer model using the optical absorption coefficient from ex-situ transmittance measurements of the as-grown samples as input parameter.

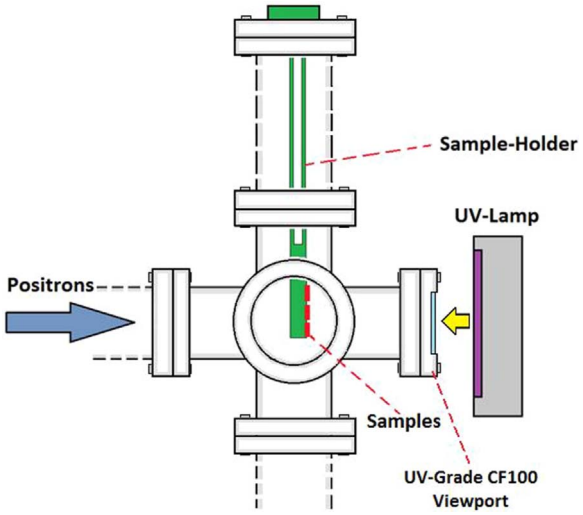

Fig. 1. Modified UHV sample chamber (base pressure =10^{-5} Pa) of the VEP Doppler broadening setup. The sample is illuminated via a UV-grade CF-100 viewport (transmittance > 90%) from the backside through the fused silica substrate, while the tunable low-energy positron beam (0.1–25 keV) probes the sample from the film side, enabling in-situ thin film depth profiling studies during UV illumination. The UV-lamp to sample distance is about 15 cm.

Prior to in-situ PAS experiments, the time dependent photochromic properties of the YO_xH_y films were probed ex-situ in air using the fibre optics spectrometer. The same illumination geometry and UV light source as shown in Fig. 1 were used to reproduce the conditions during PAS measurements and to determine reasonable time intervals for the in-situ experiments enabling the investigation of the sample in different photochromic states (see Fig. 4 below).

3. Results and discussion

3.1. Positron Doppler broadening depth profiles of Y, $YH_{1.9+\delta}$, YO_xH_y and Y_2O_3 thin films

Fig. 2 shows the Doppler S and W parameter depth profiles of Y, $YH_{1.9+\delta}$, YO_xH_y and Y_2O_3 thin films deposited on f-SiO_2 (or crystalline Si) substrates, together with the best-fit curves obtained from VEPFIT analysis. For all samples, a good contrast was obtained between the thin films probed at low positron implantation energy and the substrate probed at high positron implantation energy, enabling accurate simultaneous determination of the S and W parameters of the different yttrium-based materials. A systematic decrease of the S-parameter and simultaneous increase of W-parameter is observed along the material series Y → $YH_{1.9+\delta}$ → YO_xH_y → Y_2O_3. A quite large positron diffusion length of 47 nm was needed in the best-fit analysis of the YO_xH_y film, indicating a surface gradient in the structural or compositional properties of this particular sample.

The S and W parameter as well as the thickness of the films extracted from the VEPFIT analysis are summarized in Table 1. The mass densities given here were used as fixed input parameters. In case of Y, $YH_{1.9+\delta}$ and Y_2O_3 the bulk densities were taken, while the density of YO_xH_y is derived from ion beam analysis measurements, which will be published elsewhere.

Fig. 3 shows a S-W map where the data related to Y based samples obtained in this work are compared to the case of Mg based compounds [19,21,32]. Clearly, metallic yttrium shows the highest S-parameter whereas the W parameter has the lowest value among the compositional series Y → $YH_{1.9+\delta}$ → YO_xH_y → Y_2O_3. The S and W parameter of the metallic Y film is close to that of Mg. Furthermore, the shift in S-W

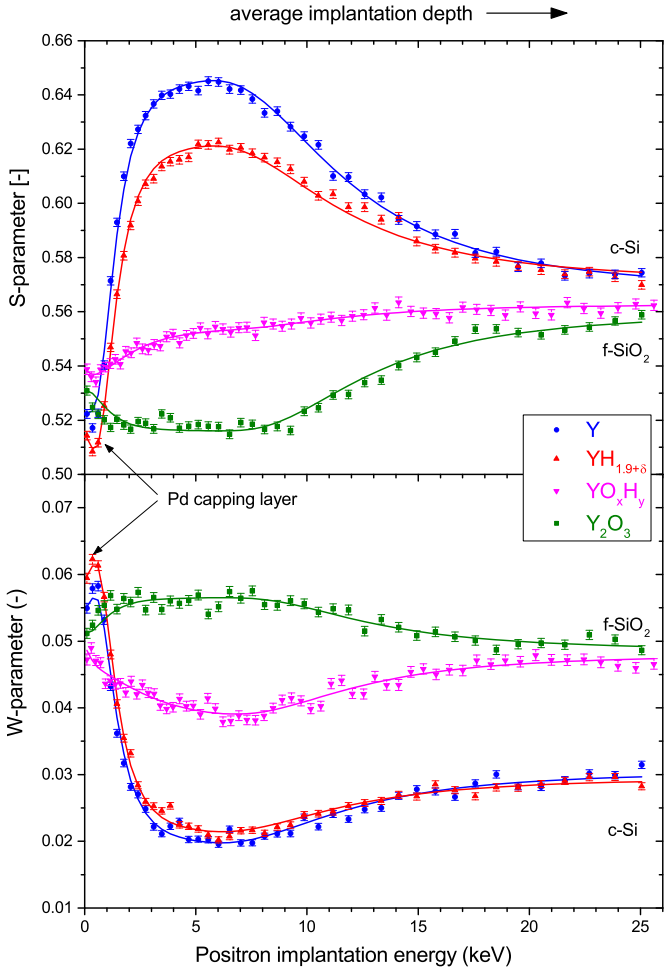

Fig. 2. Doppler Broadening PAS S and W depth profiles of Y, $YH_{1.9+\delta}$, YO_xH_y and Y_2O_3 thin films on f-SiO_2 or c-Si substrates. The full curves are best-fits obtained using VEPFIT analysis.

Table 1
Layer thickness and S and W parameter of the Y-based films obtained from VEPFIT analysis.

Film	Structure	Density (g/cm^3)	Film thickness (nm)	S parameter	W parameter
Y	$P6_3/mmc$ (hcp)	4.47	319	0.6473 ± 0.0003	0.0192 ± 0.0002
$YH_{1.9+\delta}$	Fm-3m (fcc)	4.24	321	0.6231 ± 0.0003	0.0208 ± 0.0002
Y_2O_3	I-a3 (bcc)	5.01	429	0.5159 ± 0.0002	0.0566 ± 0.0002
YO_xH_y	Cubic	4.15	479	0.5548 ± 0.0003	0.0385 ± 0.0002

upon hydrogenation to the $YH_{1.9+\delta}$ phase is very similar compared to that of Mg → MgH_2. This similarity can be understood in terms of the change of the electron momentum distribution in both cases. In metallic Y and Mg the high S parameter is caused by a dominant contribution of the conduction band electrons in Y(5 s) and Y(5p), and in M(3 s) and Mg(3p) states, respectively. These electrons mainly occupy momentum states up to a finite Fermi momentum, leading to a relatively narrow contribution to the electron momentum distribution of Y.

As hydrogen is incorporated into the yttrium lattice, metallic yttrium dihydride is formed, which is reflected in a reduction in the S parameter, caused by the formation of covalent-ionic Y-H bonds and a more localized character of the upper valence electron orbitals which broadens the electron momentum distribution [20]. This is also

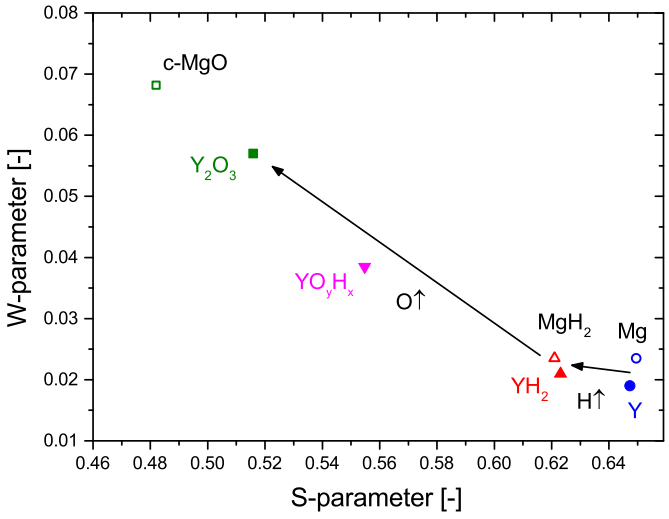

Fig. 3. S-W diagram of the S and W best-fit values for the Y, $YH_{1.9+\delta}$, YO_xH_y and Y_2O_3 thin films. For comparison, the S-W points for Mg and MgH_2 [19,21] thin films and c-MgO [32] are included. The arrows labeled by H↑ and O↑ indicate the trends upon increased hydrogen and oxygen insertion, respectively.

consistent with previous positron 1D-ACAR studies on Y and $YH_{1.9+\delta}$ [33,34] and Compton scattering studies on Mg [35] and MgH_2 [36], which show that the low momentum part of the 1D electron momentum distributions of Y and of Mg can be well described by an inverted parabola typical for a free-electron-like contribution to the electronic band structure. The extracted Fermi momenta of $5.3{\cdot}10^{-3}$ m_oc and $5.4{\cdot}10^{-3}$ m_oc for Y [33,34] and Mg [35] are very close, explaining the similar values for the S parameter seen in Fig. 3. Upon hydrogenation to the metal dihydride state, the low momentum part of the 1D electron momentum distributions can still be described quite well by an inverted parabola in the low momentum range, with larger Fermi-like momenta of $6.2{\cdot}10^{-3}$ m_oc and $6.1{\cdot}10^{-3}$ m_oc for $YH_{1.9+\delta}$ [33,34] and MgH_2 [36], respectively, leading to a similar reduction in the S-parameter, consistent with the observed shifts in S-W parameter for Y → $YH_{1.9+\delta}$ and Mg→ MgH_2 [20] (Fig. 3).

In contrast, the wide band gap (~5.6 eV) insulator yttrium oxide is characterized mainly by ionic Y^{3+}-O^{2-} bonds in which the upper valence electrons are strongly localized. This results in a rather broad electron momentum distribution typical for wide band gap oxides such as MgO and Al_2O_3, and the S-parameter shows a substantial decrease while the W-parameter increases drastically. Fig. 3 shows that upon increased hydrogen and oxygen content the S and W parameter in the sequence Y → $YH_{1.9+\delta}$ → Y_2O_3 evolve quite similar to the sequence for Mg → MgH_2 → MgO.

In contrast to Mg, Y can attain a valence of Y^{3+} or Y^{2+} depending on its chemical surroundings, *i.e.* a Y^{3+}/Y^{2+} mixed valence character can be expected, which is particularly relevant for the formation of yttrium oxy-hydrides. Semiconducting yttrium oxy-hydride with an intermediate band gap of around 2.6 eV contains both hydrogen and oxygen in its cubic crystal lattice. The S and W depth profiles lie in-between that of yttrium oxide and yttrium dihydride, reflecting the intermediate character of the electronic structure of YO_xH_y.

3.2. *Positron annihilation study of photochromic YO_xH_y films under in-situ UV illumination*

In order to examine the local structural and electronic structure changes upon photo-darkening, in-situ illumination was applied during positron annihilation studies of a set of yttrium oxy-hydride films. Fig. 4 shows the typical time dependence of optical transmittance of the YO_xH_y films due to UV illumination and subsequent bleaching in the dark at room temperature. Due to the competition of photo-darkening

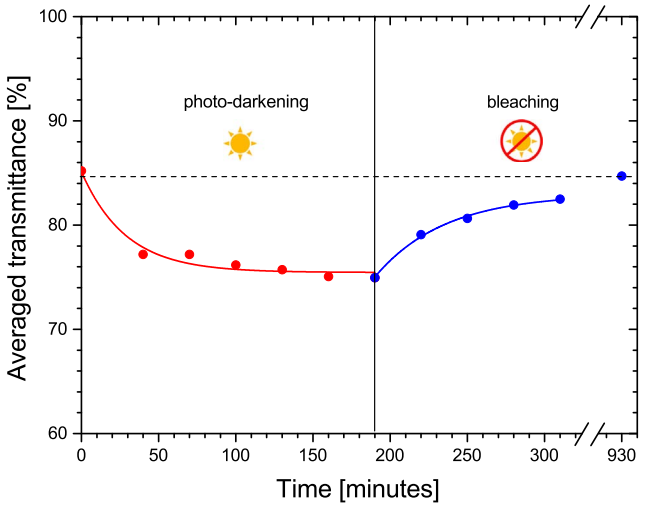

Fig. 4. Time dependence of optical transmittance averaged over the wavelength range of 500– 900 nm of a 460 nm thick YO_xH_y film on f-SiO_2 during UV-illumination and (thermal) bleaching at room temperature in the dark. A HeroLab UV lamp was used for photo-darkening.

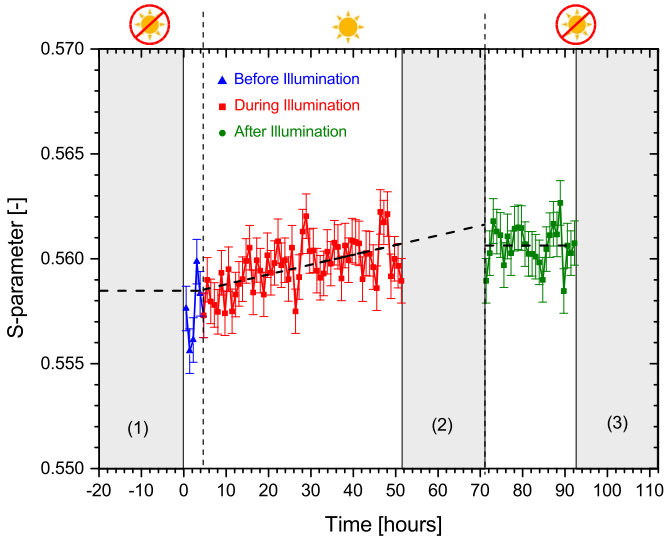

Fig. 5. Time dependence of the S parameter of a 460 nm thick photochromic YO_xH_y film #1 on f-SiO_2 substrate at fixed positron implantation energy of 7.2 keV before (blue), during (red) and after (green) UV illumination. The dashed black lines are guides-to-the-eye. During the time intervals indicated by (1), (2) and (3), full depth profiles were collected. (For interpretation of the references to color in this figure legend, the reader is referred to the web version of this article.)

and thermal bleaching processes a steady state is reached after a certain illumination duration where the transmittance becomes constant. The time required to reach this saturation value is about 2.5 h. After 15.5 h of thermal bleaching in the dark, the optical transmittance of the YO_xH_y sample returns to its original value, indicating full reversibility of the photochromic effect under these conditions. Note that under illumination with sunlight, i.e. significantly higher UV-irradiance than used in this experiment, an even faster and stronger photochromic effect is to be expected.

Fig. 5 shows the time-dependence of the S parameter of YO_xH_y sample #1 during UV illumination for 45 h and subsequent bleaching under dark conditions for 48 h, collected at a positron implantation energy of 7.2 keV. These time intervals were chosen to ensure saturation of the photochromic effect and subsequent bleaching (compare to Fig. 4). Full depth profiles were collected before and after illumination in the time intervals indicated by (1) and (3), respectively. Another full depth profile was measured *during* the last part of the illumination

Table 2
Relative change in positron Doppler S and W parameter of the YO_xH_y films upon UV illumination.

Sample	Positron energy	Illumination time	$\Delta S/S_0$	$\Delta W/W_0$
#1	Depth profile	45 h	+0.7 ± 0.1%	−0.8 ± 0.4%
#1	7.2 keV	45 h	+0.4 ± 0.15%	−0.6 ± 1%
#2	7.9 keV	48 h	+0.3 ± 0.15%	−0.8 ± 1%
#3	8.3 keV	38 h	+0.5 ± 0.1%	+0.1 ± 0.4%

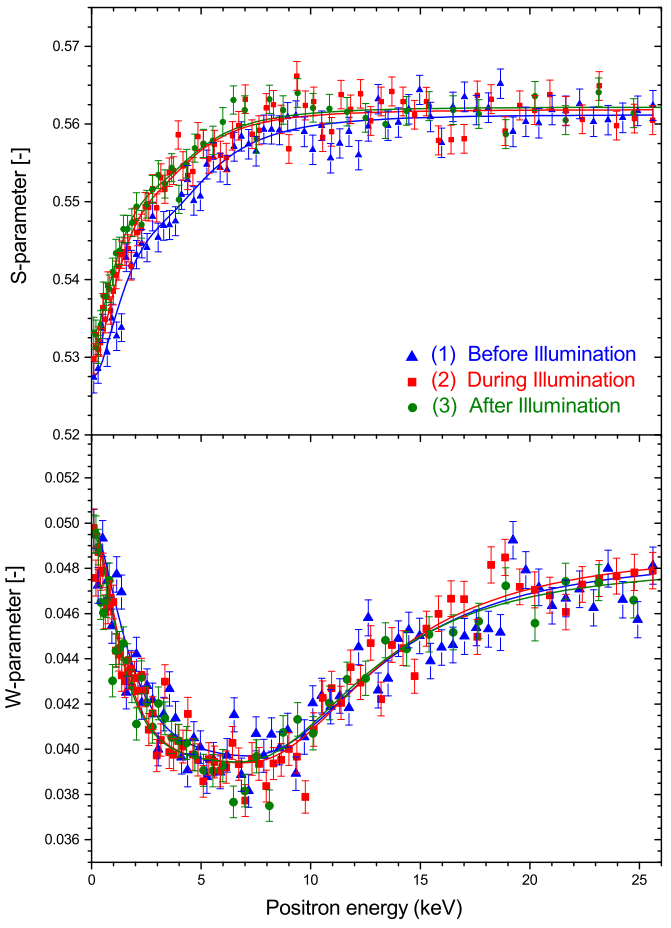

Fig. 6. S and W depth profiles of photochromic YO_xH_y sample #1 on f-SiO_2 substrate as a function of positron implantation energy before UV illumination (1), at the end of the illumination with the UV-lamp still switched on (2), and after 48 h of bleaching under dark conditions (3).

period denoted by (2). The obtained data was processed by a three-point-average in order to improve the counting statistics. A small but significant increase in S-parameter, which varies approximately linear in time, was observed systematically during photo-darkening of all YO_xH_y samples studied. Table 2 gives a summary of the changes in S and W parameter after photo-darkening. The change in W is less obvious than that of S, due to larger statistical errors caused by lower number of counts. Nevertheless, Table 2 indicates that a slight decrease in W occurs in parallel with the increase in S.

Fig. 6 presents the S and W depth profiles for the YO_xH_y sample #1 at various stages during the experiment indicated in Fig. 5, namely before the in-situ illumination experiment (1), after 45 h of illumination (2) and after 48 h of bleaching under dark conditions (3). The depth profiles show an clear increase in the S parameter and a small decrease in the W parameter after the illumination for 45 h. This confirms the corresponding time-dependent changes monitored at a fixed positron energy, i.e. single mean implantation depth, presented in Fig. 5 and in Table 2. The illumination seems to affect the entire film

with a thickness of 460 nm quite homogeneously, since a good agreement could be obtained using a single homogeneous YO_xH_y layer in the VEPFIT analysis.

3.2.1. Discussion in-situ UV illumination studies

Before examining the possible nanostructural origins in more detail, it is important to note that the comparison of depth profiles (2) and (3) in Fig. 6 shows that the changes in S and W upon UV-illumination remain constant after 48 h of bleaching under dark conditions. According to Fig. 4, the optical properties of YO_xH_y have fully reversed after ~15 h of bleaching. Therefore, it is concluded that the structural changes observed by PAS are not the same as those directly responsible for the photochromic effect. Furthermore, the nanostructural changes observed here appear to be unrelated to the reversible changes reported in the NMR study by Chandran et al. [14], where a 3% fraction of H atoms in YO_xH_y turns out to be highly mobile, and under illumination this mobility "freezes out", indicating that hydrogen finds a meta-stable binding site in the YO_xH_y structure during photodarkening. During bleaching under dark conditions, this fraction of H atoms regains a high mobility, indicating that hydrogen is directly involved in the nanostructural changes underlying the mechanism of photochromism in the YO_xH_y films. In addition, it should be noted that, since V_O (and V_H) mono-vacancies mostly are positively charged [37], positrons are not expected to trap in these anion vacancies, and are largely insensitive to the presence of these defects. Therefore, the present positron experiments do not exclude an important role of V_H and V_O anion mono-vacancies in the mechanism of the photochromic effect in yttrium oxy-hydrides.

In the following we discuss possible causes for the experimental results described above:

(i) Since the YO_xH_y films are formed by oxidation of Y-dihydride in air, further oxidation could be the reason for a shift of S and W parameters. However, we find that 14 days of post-oxidation of an yttrium oxy-hydride film in an ambient environment led to a *reduction* of S by $\Delta S/S_0 = -(1.0 \pm 0.1)\%$. This is in contrast to the observed *increase* of S during UV illumination in the VEP setup at a base vacuum of ~10^{-5} Pa. Hence, oxidation cannot explain the S and W shifts observed during in-situ PAS.

(ii) Alternatively, the change in the positron S and W parameters and corresponding modified structural/electronic properties of the YO_xH_y films could be related to the so-called memory effect that is related to the photochromism of yttrium oxy-hydrides [12], in which an enhanced change in transmittance is observed in the 2nd and further photochromic cycles, while the bleaching kinetics is slowed down. This memory effect is claimed to be metastable, and is reported to last as long as a few weeks. In future studies, it will thus be important to investigate whether the positron annihilation parameters are related to the metastable structural transformations underlying the memory effect, by monitoring the positron parameters on a time-scale compatible with the time-scale of fading of the memory effect, i.e. several weeks.

(iii) Finally, the non-reversible changes in S and W parameter might be related to heat-induced effects causing changes in the defect structure of YO_xH_y. In the following section thermal effects are investigated in more detail. It is demonstrated that temperature induced effects in S and W become significant only above about 90 °C. Hence, due to the very low optical power of the UV lamp of only (590 ± 50) μW/cm^2 temperature effects during UV-illumination seem to be rather implausible.

The increase in S and decrease in W during in-situ PAS experiments indicates the formation of vacancies during UV-illumination. Trapping of positrons in neutral or negatively charged vacancies leads to less overlap with high-momentum core electrons. This is because the valence electron orbitals of the surrounding atoms extend farther into the open space where the positron resides than the core electron orbitals. This leads to a higher probability of annihilation with low-momentum electrons, and thus, to a higher S parameter together with a lower W parameter. It is instructive to compare the observed changes to typical values for the shift in S and W upon formation of cation monovacancies. For example, saturation trapping in Zn monovacancies in c-ZnO leads to substantially larger shifts of $\Delta S/S_{c\text{-}ZnO} \sim +5.5\%$ and $\Delta W/W_{c\text{-}ZnO} \sim -19\%$ [22,23,38]. The small changes in S and W given in Table 2 therefore indicate that the concentration of generated cation vacancies is relatively low. The observed structural changes most likely correspond to either the formation of cation vacancies, as argued above, or to the association of mono-vacancies into small vacancy clusters. The formation of larger (neutral) vacancy clusters (such as V_Y-V_H or V_O-V_H divacancies) by clustering of generated anion mono-vacancies to already present vacancies in the YO_xH_y films would lead to sufficiently large and neutral open space to trap positrons. This will certainly lead to an increase in S, but the corresponding change in the W parameter will be less than for the case of formation of isolated cation vacancies. This corresponds better with the observed changes in S and W. The positron data thus point to the formation of small vacancy clusters such as V_H-V_H, V_Y-V_H or V_O-V_H, induced by e.g. dissociation of loosely bonded H which subsequently moves away, rather than to the formation of isolated cation vacancies V_Y. However, it appears that these vacancy clusters do not directly cause the photochromism.

3.3. Thermal effects on the positron Doppler broadening parameters of YO_xH_y

In an earlier stage of our studies, we employed a QTH (Quartz Tungsten Halogen) lamp placed inside the sample chamber of the VEP setup for the in-situ positron annihilation studies. The QTH lamp was placed at a close distance of ~1.5 cm to the photochromic sample in a back-illumination geometry.

A thermocouple was mounted in thermal contact to the sample. In these experiments, high-power in-situ illumination inside the evacuated sample chamber led to substantial heating of the sample, up to temperatures of ~130 °C and increasing linearly with QTH lamp power in the range up to 70 W. This effect is mainly due to the strong infrared emission of the QTH lamp, which is absorbed by the fused silica substrate. The positron annihilation studies revealed that such thermal heating has a pronounced effect on the S-W parameters for temperatures above ~90 °C.

Fig. 7 presents the time-dependence of the S and W parameter monitored at a mean positron implantation depth at the centre of a 429 nm thick YO_xH_y film, during 45 W QTH illumination for 1.5 h and during the time interval after the illumination. At this lamp power a final sample temperature of 96 °C is reached after about 90 min. Clearly, the S parameter increases during the illumination and remains constant after the illumination is stopped. The W-parameter shows an opposite trend and decreases during the illumination. The evolution of the S and W parameters occurs on a similar time scale as the temperature of the sample over time, which increases rapidly to a temperature of ~80 °C during the first 20 min and stabilizes at a final temperature of ~96 °C after about 90 min. This variation in the positron parameters points to the formation of vacancies, possibly by hydrogen which is liberated from Y-H bonds.

The complete S and W depth profiles collected before and after the QTH heat treatment showed that the S-parameter increases quite significantly by $\Delta S/S_0 = +1.3\%$, while the W-parameter decreases by $\Delta W/W_0 = -2\%$. The S-parameter remains at an increased value for at least 25 days (Fig. 7), showing the permanent nature of the structural changes. In the case of a sample temperature of 130 °C (70 W), substantially larger permanent changes are seen of $\Delta S/S_0 = +8.2\%$ and $\Delta W/W_0 = -8\%$ (see also Fig. 9).

Fig. 8 presents the shift in the S parameter, ΔS, as a function of final

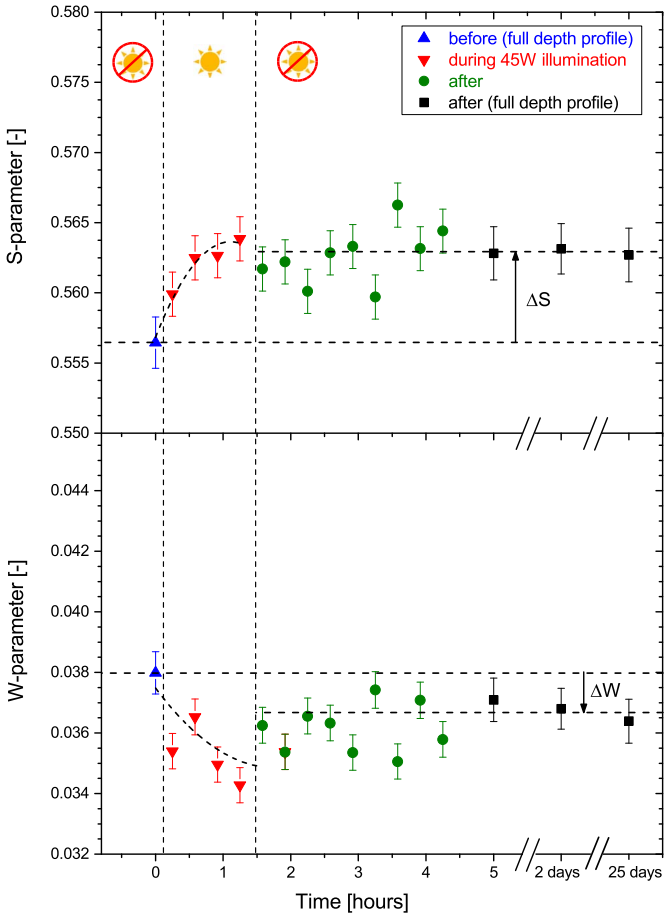

Fig. 7. : (Color online only). Time dependence of the S and W parameter monitored at a fixed positron implantation energy of 6 keV during (red) and after (green) heating to T~96 °C by 45 W illumination with a QTH lamp inside the sample chamber for a photochromic YO_xH_y film on f-SiO_2. The blue and black data points correspond to VEPFIT fitting results obtained from full PAS depth profiles acquired before and several days after the in-situ illumination. The dashed curves serve as a guide-to-the-eye. (For interpretation of the references to color in this figure legend, the reader is referred to the web version of this article.)

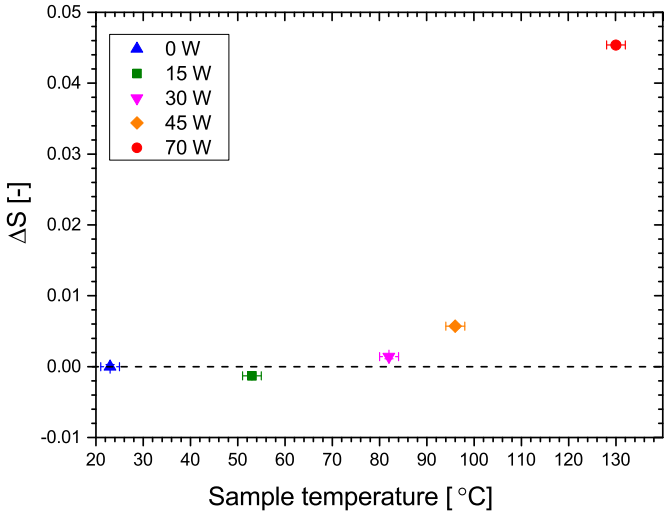

Fig. 8. Change in S parameter, ΔS, as a function of final sample temperature of YO_xH_y films on f-SiO_2 substrates induced by QTH illumination for 1.5 h at various lamp powers.

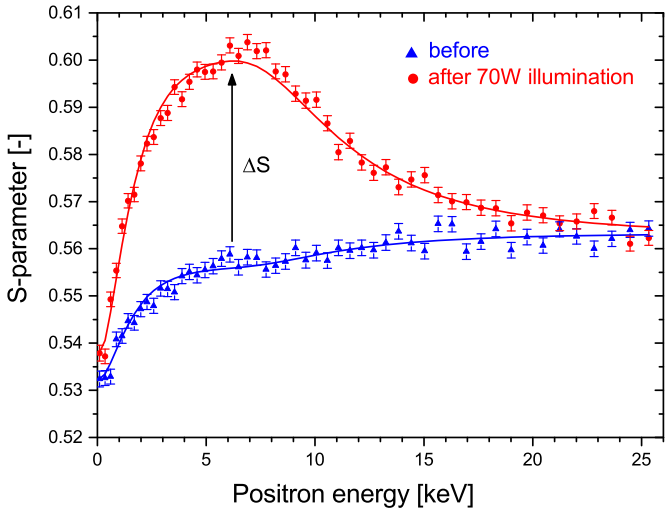

Fig. 9. Doppler S parameter depth profiles before and after the 1.5 h heat treatment at 130 °C (70 W).

sample temperature, T, demonstrating that significant changes in the S parameter are only observed at temperatures above about 90 °C. The relative change in W of $\Delta W/W_0 = -8\%$ (about the same in size as $\Delta S/S_0 = +8.2\%$) seems too small to be caused by cation monovacancy formation, but can be due to clustering of vacancies, e.g by the formation of V_Y-V_H, V_H-V_H or V_H-V_O divacancies. Possibly, in the temperature range above 90 °C, breaking of Y–H bonds in the film leads to the formation of hydrogen vacancies and hydrogen interstitials which might effuse out of the film, leaving the vacancy-related defects behind. Another possible explanation for the thermally induced drastic changes of the S parameter could be the formation of metallic Y or Y dihydride based nano-clusters. However, the slope in the S-W plot corresponding to the thermal effects is $R = \Delta W\%/\Delta S\% \approx -1$, whereas the slope corresponding to the composition change from $YO_xH_y \rightarrow YH_{1.9+\delta} \rightarrow Y$ is $R = -50\%/14\% \approx -3.5$. This indicates that positron trapping in Y or YH_x clusters can be excluded here. Therefore, the most probable cause for the changes in S and W upon thermal treatment thus seems to involve the formation of hydrogen vacancies and a subsequent clustering into divacancies or small multivacancies.

The inferred low temperature H effusion is puzzling, since hydrogen is quite strongly bonded in the $YH_{1.9+\delta}$ phase, with very low desorption pressures of the order of $\sim 10^{-4}$ Pa at room temperature [39–41]. Possibly, the presence of trace amounts of oxygen might lead to the desorption of water. In the current study, a highly reactive YO_xH_y surface is present for the uncapped photochromic films. H effusion in the defect-rich yttrium oxy-hydride films might occur at a relatively low temperature. It would be interesting to investigate whether this leads to desorption of water or hydrogen by *e.g.* thermal desorption spectroscopy [42,43].

Additional optical transmittance measurements showed that the band gap of the thermally treated YO_xH_y films does not change up to 96 °C (45 W QTH-lamp power). A substantial band-gap increase from 2.53 eV to (2.78 ± 0.04) eV correlated with the S-W shifts was observed in the case of T=130 °C (70 W QTH-lamp power). This indicates an increased O:H ratio, as the more ionic character of electron orbitals related to Y–O bonds will become more dominant and a correspondingly larger optical band gap may result.

Interestingly, no structural changes could be observed by standard X-ray diffraction (XRD) as the fcc diffraction peak positions and intensities remained the same within experimental errors. This supports the proposed vacancy formation involving (local) H removal in an otherwise similar crystal structure as the prime atomic-scale process induced by the heat treatment.

4. Conclusions

The presented positron Doppler broadening study showed that the electron momentum distribution changes substantially in the sequence Y → $YH_{1.9+\delta}$ →Y_2O_3, reflecting the differences in the electronic structure of a metal with a free-electron-like contribution, a metal with covalent-ionic Y–H bonds, and an ionic wide band gap insulator, respectively. The changes in the low momentum valence electron distributions are quite similar to those observed for the sequence Mg→MgH_2→MgO. The transparent semiconductor YO_xH_y with a band gap of ~2.6 eV is characterized by positron annihilation S and W parameters which are intermediate those of $YH_{1.9+\delta}$ and Y_2O_3, reflecting the effects of the incorporated oxygen and possibly of Y^{2+}/Y^{3+} mixed valence character in the YO_xH_y system. The observed variation in the electronic structure properties in the sequence Y, $YH_{1.9+\delta}$, YO_xH_y and Y_2O_3 is in line with previous ab-initio calculations and insights gained from optical spectroscopy, Compton scattering and positron 2D-ACAR studies. 2D-ACAR studies of the electron momentum distributions of $YH_{1.9+\delta}$ and YO_xH_y combined with ab-initio modelling seem promising to gain detailed insights into their electronic structure.

In-situ illumination with UV light induces photo-darkening of the YO_xH_y films. This leads to a small increase in the S parameter and a decrease in W. Possibly these changes are related to the generation of small concentrations of cation vacancies or to the association of generated anion vacancies and cation vacancies into small vacancy clusters. The observed structural changes do not reverse on the time-scale of bleaching under dark conditions, and therefore do not play a direct role in the mechanism of the photochromic effect. Nevertheless, they could be at the basis of the (meta-stable) memory effect in the photochromism of YO_xH_y. Future positron annihilation lifetime spectroscopy studies could identify the size of the vacancy clusters formed, and provide insights into the corresponding concentrations. The current study does not exclude H mono-vacancies (V_H) or O mono-vacancies (V_O) as a key player in the photochromic effect of YO_xH_y films, since these vacancies are likely positively charged in equilibrium and thus would not trap positrons effectively.

Thermal annealing of YO_xH_y films above 90 °C leads to pronounced formation of vacancies, including divacancies or small multivacancies with a predominance of anion vacancies, most likely associated with the breaking of weakly bonded hydrogen atoms. The simultaneous widening of the optical band gap indicates increased O:H atomic ratios. Consequently, some hydrogen may effuse and possibly even desorb from the film due to the reactivity of the bare YO_xH_y surface. Here, follow-up studies based on e.g. thermal desorption spectroscopy and NMR could provide deeper insights into the role and evolution of hydrogen.

Acknowledgements

This research is supported by the Dutch Technology Foundation STW, which is part of the Netherlands Organisation for Scientific Research (NWO), and which is partly funded by the Ministry of Economic Affairs. We thank M. de Boer and Dr. M. Butterling for technical assistance in the positron annihilation studies including in-situ UV illumination, and K. Goubitz for assistance in the X-ray diffraction measurements.

References

[1] A. Gavrilyuk, Photochromism in WO_3 thin films, Electrochim. Acta 44 (1999) 3027–3037.
[2] G.A. Niklasson, C.G. Granqvist, Electrochromics for smart windows: thin films of tungsten oxide and nickel oxide, and devices based on these, J. Mater. Chem. 17 (2007) 127–156.
[3] S.K. Deb, Optical and photoelectrical properties and colour centres in thin films of tungsten oxide, Philos. Mag. 27 (1973) 801–822.
[4] C.G. Granqvist, Handbook of Inorganic Electrochromic Materials, Elsevier, Amsterdam, 1995.
[5] J.N. Huiberts, R. Griessen, J.H. Rector, R.J. Wijngaarden, J.P. Dekker, D. de Groot, N.J. Koeman, Yttrium and lanthanum hydride films with switchable optical properties, Nature 380 (1996) 231–234.
[6] R. Griessen, Switchable Mirrors, Europhys. News 32 (2001) 41–44.
[7] K. Yoshimura, C. Langhammer, B. Dam, Metal hydrides for smart window and sensor applications, MRS Bull. 38 (2013) 495–503.
[8] P. van Gelderen, P.A. Bobbert, P.J. Kelly, G. Brocks, Parameter-free quasiparticle calculations for YH_3, Phys. Rev. Lett. 85 (2000) 2989–2992.
[9] M. Kremers, N.J. Koeman, R. Griessen, P.H.L. Notten, R. Tolboom, P.J. Kelly, P.A. Duine, Optical transmission spectroscopy of switchable yttrium hydride films, Phys. Rev. B 57 (1998) 4944–4949.
[10] A.F.Th. Hoekstra, A.S. Roy, T.F. Rosenbaum, R. Griessen, R.J. Wijngaarden, N.J. Koeman, Light-induced metal-insulator transition in a switchable mirror, Phys. Rev. Lett. 86 (2001) 5349–5352.
[11] A. Ohmura, A. Machida, T. Watanuki, K. Aoki, S. Nakano, K. Takemura, Photochromism in yttrium hydride, Appl. Phys. Lett. 91 (2007) 151904-1–151904-3.
[12] T. Mongstad, C. Platzer-Björkman, J.P. Maehlen, L.P.A. Mooij, Y. Pivak, B. Dam, E.S. Marstein, B.C. Hauback, S.Zh. Karazhanov, A new thin film photochromic material: oxygen-containing yttrium hydride, Sol. Energy Mater. Sol. Cells 95 (2011) 3596–3599.
[13] T. Mongstad, C. Platzer-Björkman, S.Zh. Karazhanov, A. Holt, J.P. Maehlen, B.C. Hauback, Transparent yttrium hydride thin films prepared by reactive sputtering, J. Alloy. Compd. 509S (2011) S812–S816.
[14] C.V. Chandran, H. Schreuders, B. Dam, J.W.G. Janssen, J. Bart, A.P.M. Kentgens, P.J.M. van Bentum, Solid-State NMR studies of the photochromic effects of thin films of oxygen-containing yttrium hydride, J. Phys. Chem. C. 118 (2014) 22935–22942.
[15] A. Pishtshev, S. Karazhanov, Role of oxygen in materials properties of yttrium hydride, Solid State Commun. 194 (2014) 39–42.
[16] C.C. You, T. Mongstad, J.P. Maehlen, S. Karazhanov, Engineering the band gap and optical properties of thin films of yttrium hydride, Appl. Phys. Lett. 105 (2014) 031910.
[17] S.B. Dugdale, H.M. Fretwell, M.A. Alam, G. Kontrym-Sznajd, R.N. West, S. Badrzadeh, Direct observation and calipering of the "Webbing" Fermi surface of yttrium, Phys. Rev. Lett. 79 (1997) 941–944.
[18] G. Kontrym-Sznajd, M. Samsel-Czekała, A. Pietraszko, H. Sormann, S. Manninen, S. Huotari, K. Hämäläinen, J. Laukkanen, R.N. West, W. Schülke, Electron momentum density in yttrium, Phys. Rev. B 66 (2002) 155110.
[19] S.W.H. Eijt, R. Kind, S. Singh, H. Schut, W.J. Legerstee, R.W.A. Hendrikx, V.L. Svetchnikov, R.J. Westerwaal, B. Dam, Positron depth profiling of the structural and electronic structure transformations of hydrogenated Mg-based thin films, J. Appl. Phys. 105 (2009) 043514.
[20] S.W.H. Eijt, Meeting challenges in nanomaterials for sustainable energy applications using high-resolution positron methods, Physica Status Solidi (C.) 6 (2009) 2561–2565.
[21] S.W.H. Eijt, H. Leegwater, H. Schut, A. Anastasopol, W. Egger, L. Ravelli, C. Hugenschmidt, B. Dam, Layer-resolved study of the Mg to MgH_2 transformation in Mg-Ti films with short-range chemical order, J. Alloy. Compd. 509S (2011) S567–S571.
[22] F. Tuomisto, I. Makkonen, Defect identification in semiconductors with positron annihilation: experiment and theory, Rev. Mod. Phys. 85 (2013) 1583–1631.
[23] I. Makkonen, E. Korhonen, V. Prozheeva, F. Tuomisto, Identification of vacancy defect complexes in transparent semiconducting oxides ZnO, In_2O_3 and SnO_2, J. Phys.: Condens. Matter 28 (2016) 224002.
[24] H. Leegwater, H. Schut, W. Egger, A. Baldi, B. Dam, S.W.H. Eijt, Divacancies and the hydrogenation of Mg-Ti films with short range chemical order, Appl. Phys. Lett. 96 (2010) 121902.
[25] W. Brandt, H.F. Waung, P.W. Levy, Positron Annihilation Centers in NaCl, Phys. Rev. Lett. 26 (1971) 496–499.
[26] K. Asano, R.J. Westerwaal, A. Anastasopol, L.P.A. Mooij, C. Boelsma, P. Ngene, H. Schreuders, S.W.H. Eijt, B. Dam, Destabilization of Mg hydride by the formation of nanometer-sized clusters in the immiscible Mg-Ti system, J. Phys. Chem. C. 119 (2015) 12157–12164.
[27] M.A. van Huis, A. van Veen, H. Schut, C.V. Falub, S.W.H. Eijt, P.E. Mijnarends, J. Kuriplach, Positron confinement in embedded lithium nanoclusters, Phys. Rev. B 65 (2002) 085416.
[28] C.V. Falub, P.E. Mijnarends, S.W.H. Eijt, M.A. van Huis, A. van Veen, H. Schut, Electronic structure and orientation relationship of Li nanoclusters embedded in MgO studied by depth selective positron annihilation two-dimensional angular correlation, Phys. Rev. B 66 (2002) 075426.
[29] Y. Nagai, M. Hasegawa, Z. Tang, A. Hempel, K. Yubuta, T. Shimamura, Y. Kawazoe, A. Kawai, F. Kano, Positron confinement in ultrafine embedded particles: quantum-dot-like state in an Fe-Cu alloy, Phys. Rev. B 61 (2000) 6574–6578.
[30] A. van Veen, H. Schut, J. de Vries, R.A. Hakvoort, M.R. IJpma, Analysis of positron profiling data by means of VEPFIT, AIP Conf. Proc. 218 (1991) 171–196.
[31] A. van Veen, H. Schut, P.E. Mijnarends, Depth-profiling of subsurface regions, interfaces and thin films, in: P.G. Coleman (Ed.)Positron Beams and Their Applications, World Scientific, Singapore, 2000, pp. 191–225.
[32] S.W.H. Eijt, J. de Roode, H. Schut, B.J. Kooi, J.Th.M. de Hosson, Formation and stability of rock salt ZnO nanocrystals in MgO, Appl. Phys. Lett. 91 (2007) 201906.
[33] B. Rozenfeld, E. Debowska, Investigation of electronic-structure of yttrium hydrides by positron annihilation, Acta Physica Pol. A 47 (1975) 37–43.
[34] I.Ya. Dekhtyar, V.I. Shevchenko, Positron annihilation in hydrides of transition metals, Physica Status Solidi (b) 83 (1977) 323–330.

[35] M. Brancewicz, H. Reniewicz, A. Andrejczuk, L. Dobrzyński, E. Żukowski, S. Kaprzyk, Electron momentum density of hexagonal magnesium studied by Compton scattering, Solid State Phenom. 112 (2006) 123–132.
[36] J. Felsteiner, M. Heilper, I. Gertner, A.C. Tanner, R. Opher, K.-F. Berggren, Compton scattering study of the electronic structure of magnesium hydride, Phys. Rev. B 23 (1981) 5156–5162.
[37] W. Wang, A. Janotti, C.G. van de Walle, Role of oxygen vacancies in crystalline WO_3, J. Mater. Chem. 4 (2016) 6641–6648.
[38] E.H. Kahn, M.H. Weber, M.D. McCluskey, Formation of isolated Zn vacancies in ZnO single crystals by absorption of ultraviolet radiation: a combined study using positron annihilation, photoluminescence, and mass spectroscopy, Phys. Rev. Lett. 111 (2013) 017401.
[39] E.S. Kooij, A.T.M. van Gogh, D.G. Nagengast, N.J. Koeman, R. Griessen, Hysteresis and the single-phase metal-insulator transition in switchable YH_x films, Phys. Rev. B 62 (2000) 10088–10100.
[40] A.T.M. van Gogh, D.G. Nagengast, E.S. Kooij, N.J. Koeman, J.H. Rector, R. Griessen, C.F.J. Flipse, R.J.J.G.A.M. Smeets, Structural, electrical, and optical properties of $La_{1-z}Y_zH_x$ switchable mirrors, Phys. Rev. B 63 (2001) 195105.
[41] Y. Pivak, H. Schreuders, B. Dam, Effect of the structure transformation on the (de) hydrogenation hysteresis of $La_{1-z}Y_zH_x$ films as studied by hydrogenography, J. Mater. Chem. 22 (2012) 24453–24462.
[42] V. Vons, H. Leegwater, W.J. Legerstee, S.W.H. Eijt, A. Schmidt-Ott, Hydrogen storage properties of spark generated palladium nanoparticles, Int. J. Hydrog. Energy 35 (2010) 5479–5489.
[43] V.A. Vons, A. Anastasopol, W.J. Legerstee, F.M. Mulder, S.W.H. Eijt, A. Schmidt-Ott, Low temperature hydrogen desorption and the structural properties of spark discharge generated Mg nanoparticles, Acta Mater. 59 (2011) 3070–3080.
[44] American Society for Testing and Materials (ASTM), Terrestrial Reference Spectra for Photovoltaic Performance Evaluation, ASTM G173-03, global tilt, ⟨http://rredc.nrel.gov/solar/spectra/am1.5/⟩.